Novel 5-Substituted Oxindoles Derivatives as Bruton's Tyrosine Kinase Inhibitors: Design, Synthesis, Docking, Molecular Dynamic Simulation, and Biological Evaluation

Vani Madhuri Velavalapalli,[a,b] Venkatanarayana Chowdary Maddipati,[b] Soňa Gurská,[c,d] Narendran Annadurai[c], Barbora Lišková,[c] Naresh Kumar Katari,[b] Petr Džubák,[c,d] Marián Hajdúch,[c,d] Viswanath Das,*[c,d] Rambabu Gundla,*[b]

[a] GITAM School of Pharmacy, GITAM Deemed to be University, Hyderabad, Telangana-502329, India

[b] Department of Chemistry, GITAM School of Science, GITAM Deemed to be University, Hyderabad, Telangana-502329, India

[c] Institute of Molecular and Translational Medicine, Faculty of Medicine and Dentistry, Palacký University and University Hospital Olomouc, Hněvotínská 1333/5, 77900 Olomouc, Czech Republic

[d] Czech Advanced Technologies and Research Institute (CATRIN), Institute of Molecular and Translational Medicine, Palacký University Olomouc, Olomouc, Czech Republic

∗ Corresponding authors
Viswanath Das (Email: viswanath.das@upol.cz, Tel.: +420 585 632 111)
Rambabu Gundla (Email: rgundla@gitam.edu, Tel.: +91-9849869933)

Highlights

- 3- Substituted Oxindoles were designed and evaluated as BTK inhibitors.
- Molecular dynamic simulations were carried out to understand the protein-ligand interactions.
- 9b, 9f, 9g, and 9h inhibited BTK-high Burkitt's lymphoma cells with IC_{50} values below 3 μM.
- 9h inhibited pBTK (Tyr223) activity and is a promising candidate for further modifications as a promising anti-BTK agent.

Graphical Abstract

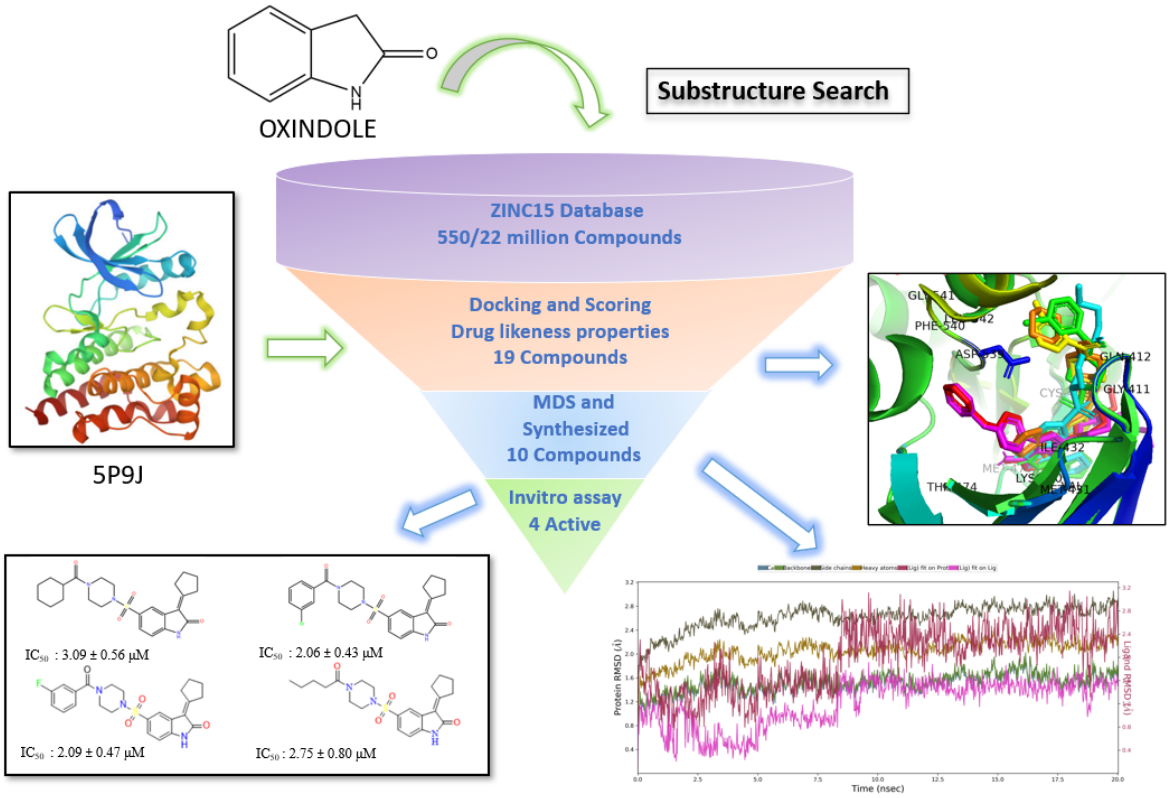

Abstract

Bruton's tyrosine kinase (BTK) is a non-RTK cytoplasmic kinase predominantly expressed by haemopoietic lineages, particularly B-cells. A new Oxindole-based focused library was designed to identify potent compounds targeting the BTK protein as anticancer agents. This study used rational approaches like structure-based pharmacophore modelling, docking, and ADME properties to select compounds. The Molecular dynamics simulation analysis carried out at 20 ns supported the stability of compound **9g** within the binding pocket. All the compounds were synthesized and subjected to biological screening on two BTK-expressing cancer cell lines, RAMOS and K562, and six non-BTK cancer cell lines, A549, HCT116 (parental and $p53^{-/-}$), U2OS, JURKAT, and CCRF-CEM, and two non-malignant cell lines, BJ and MRC-5. This study resulted in the identification of four new compounds, **9b**, **9f**, **9g**, and **9h**, which displayed potent activity against BTK-high RAMOS cells. These four compounds, each possessing free binding energies of -10.8, -11.1, -11.3, and -10.8 Kcal/mol, demonstrated antiproliferative and cytotoxic effects in RAMOS cells with IC_{50} values falling within the lower sub-micromolar range.

Keywords: Antiproliferative activity; Burkitt's lymphoma; Bruton's tyrosine kinase; Molecular dynamics simulation; RAMOS cells; Oxindoles.

Introduction

Bruton's tyrosine kinase (BTK) belongs to the Tec family of kinase and is a non-RTK cytoplasmic kinase primarily expressed by haemopoietic lineages, particularly B-cells [1]. BTK has five different domains: the PH (Pleckstrin Homology) domain acts as a membrane localization module by binding to phosphoinositide phospholipids; the TH (Tec Homology) domain contains a zinc-finger motif for the stability of the protein; SH3 (SRC homology) contains Y223; SH2 (SRC homology) domain binds to phosphorylated tyrosinase and proline-rich regions involved in protein-protein interactions; and SH-1 (Kinase or catalytic) domain contain Y551 where it is phosphorylated by Spleen tyrosine kinase (SYK) or LYN Proto-Oncogene (LYN) [2] shown in **Figure 1.** BTK is also activated when PIP3/PI3K is attached to the PH domain with different cell surface receptors [3,4]. The B-cell malignancies include chronic lymphocytic leukaemia (CLL), follicular lymphoma (FL), Waldenström's macroglobulinemia (WM), Mantle cell lymphoma (MCL), diffuse large B-cell lymphoma [5]. Recently, many studies have shown that BTK is the target for non-Hodgkin's lymphomas (NHL), specifically CLL, BCL, and autoimmune diseases [6]. There are three marketed oral BTK inhibitors: ibrutinib, zanubrutinib, and acalabrutinib [5]. Ibrutinib is an irreversible BTK inhibitor for treating CLL, MCL, and WM [7]. Zanubrutinib is used for adult patients with MCL after one prior therapy [8]. Acalabrutinib is used for MCL, CLL, and small lymphocytic lymphoma (SLL) [9]. Some BTK inhibitors under study are branebrutinib, HM71224, DTRMWXHS-12 DTRM, PRN-1008, ONO/GS-4059, spebrutinib, and ARQ-531 [5].

Oxindole is the scaffold of the compounds with potential clinical applications in drug discovery [10-12]. Importantly, substituted oxindole derivatives exhibit selectivity towards protein kinases, VEGFR being the most investigated target [13-15]. A few critical US FDA-approved drugs that contain indoline-2-one are sunitinib, toceranib phosphate, and nitedanib. For GIST advanced renal cell carcinoma, sunitinib works by inhibiting multiple receptor tyrosine kinases [16]. Toceranib Phosphate for mast cell tumours [17]. Nitedanib, an inhibitor of intracellular tyrosine kinase, for idiopathic pulmonary fibrosis and non-small cell lung cancers [18]. Several other oxindole derivatives, such as ropinirole, adibendan, indolidan, and ziprasidone, have been successfully developed as marketed drugs for various medical conditions [19-22] **(Figure 2).**

Until now, the market has predominantly featured irreversible BTK inhibitors. Nonetheless, reversible BTK inhibitors hold greater appeal due to their potential to reduce off-target side effects and mitigate resistance associated with the amino acid CYS-481 [5]. Therefore, tremendous efforts have been devoted to developing novel BTK inhibitors that are effective, selective, and safe.

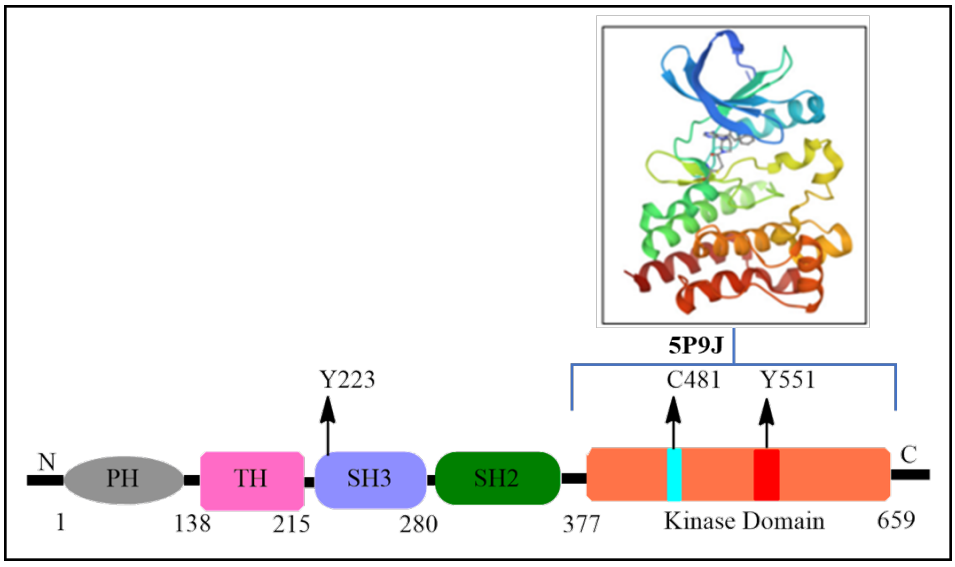

Figure 1. A graphical depiction of the sequence and homology of BTK.

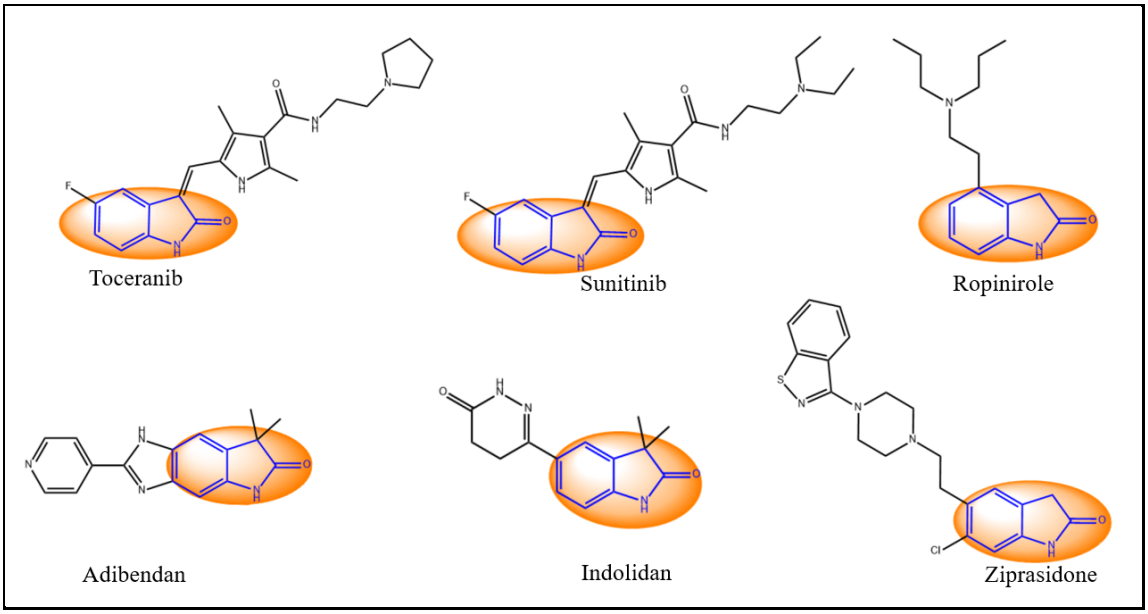

Figure 2. Few marketed drugs have oxindole as the core moiety.

Results and Discussion

Structure-based designing was carried out to generate anticancer compounds against BTK protein **(Figure 3)**. Initially, Compound **819** was identified as the lead compound from the docking based on the binding free energy and further modifications were carried out to increase its interactions with the critical amino acids in BTK (PDB-5P9J), as shown in **Figure 4.** For the purpose of establishing a structure-activity relationship, acid chlorides were introduced at position R (**Scheme 1**), leading to the synthesis of ten compounds. It is worth noting that all ten compounds exhibited favorable ADME properties, as detailed in Table 1.

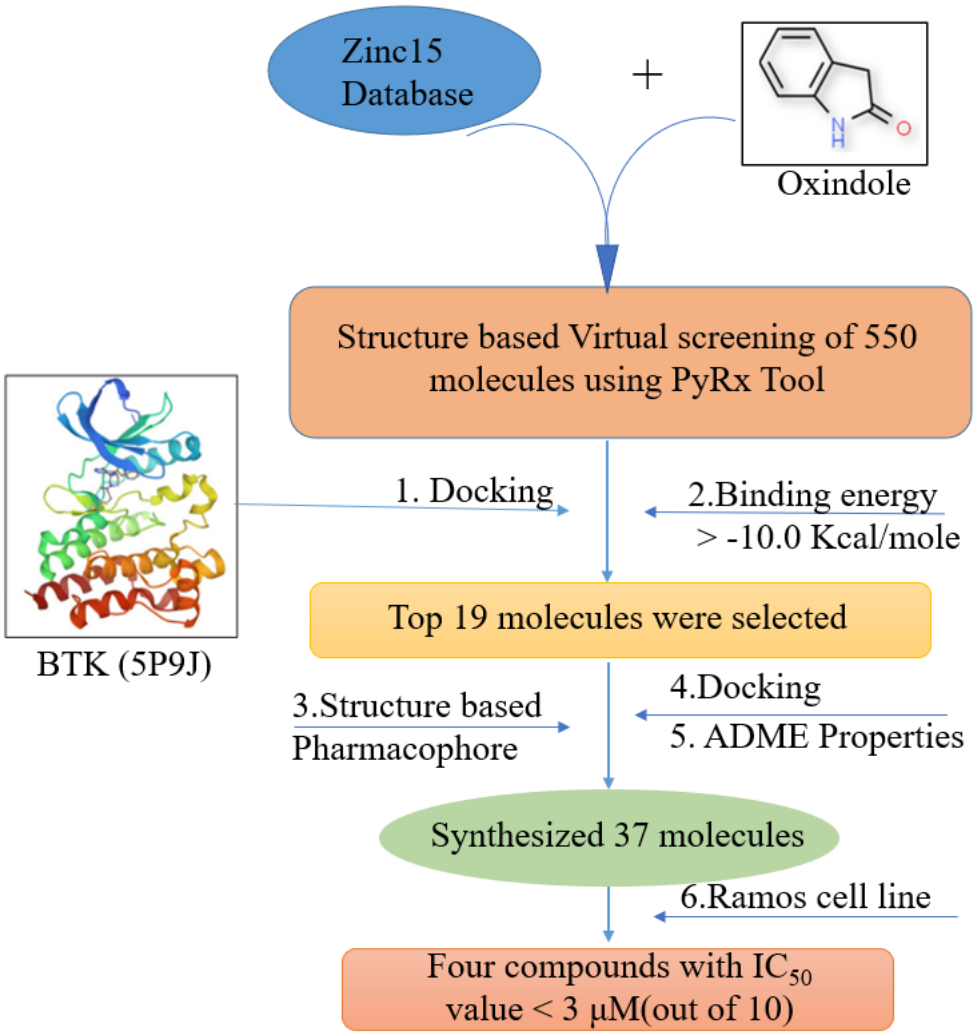

Figure 3. Schematic representation of workflow of the study.

Table 1. ADME properties of the ten compounds from Swiss ADME, along with the docking score.

Molecules	MW	TPSA	iLOGP	BBB permeant	Lipinski #violations	MR	Free energy binding (Kcal/Mol)	# Hydrogen bond acceptor	#Hydrogen bond donor
9a	412.52	95.17	3.15	No	0	122.42	-10.7	5	1
9b	457.59	95.17	3.28	No	0	134.73	-10.8	5	1
9c	415.51	95.17	2.99	No	0	120.31	-10.5	5	1
9d	451.54	95.17	3.05	No	0	132.71	-11.1	5	1
9e	485.98	95.17	3.00	No	0	137.72	-11.1	5	1
9f	530.43	95.17	3.37	No	1	140.41	-11.4	5	1
9g	469.53	95.17	2.90	No	0	132.67	-11.3	6	1
9h	431.55	108.06	2.41	No	0	130.51	-10.8	5	1
9i	452.53	95.17	3.48	No	0	127.23	-10.7	6	1
9j	519.54	95.17	2.99	No	1	137.71	-10.5	8	1
Co-Crystal	-	-	-	-	-	-	-9.5	-	-

The methyl benzyl group attached to the piperazine ring was replaced with the different acid chlorides, which showed interaction with ASP-539 amino acid and GLN-412. Replacing the methyl group with hydrogen in the piperazine ring and the oxindole ring methyl group with hydrogen showed better interaction with MET-477 and LEU-528 at the base of the ATP pocket **(Figure 4).** The amino acid MET-477 forms a hydrogen bond with the carbonyl oxygen of the oxindole ring, and LEU-528 forms a Pi-sigma bond with the phenyl of the oxindole ring in the H1 pocket **(Figure 5).** The amino acids VAL-416, ALA-428, and LEU- 408 form alkyl and pi-alkyl bonds with an oxindole ring in the H1 pocket. Other amino acids CYS-481, GLY- 480, ALA-478, TYR-476, THR-474, and GLU-475 form Vander Waals interactions with the cyclopentylidene moiety in the H2 lipophilic pocket. The amino acid ASN-526 forms a carbon-hydrogen bond with the piperazine ring, oriented towards the bottom of the H3 pocket **(Figure 5).** In the H3 pocket, we changed ten different acid chloride substitutions and synthesized analogues with docking scores of more than -10 Kcal/mol.

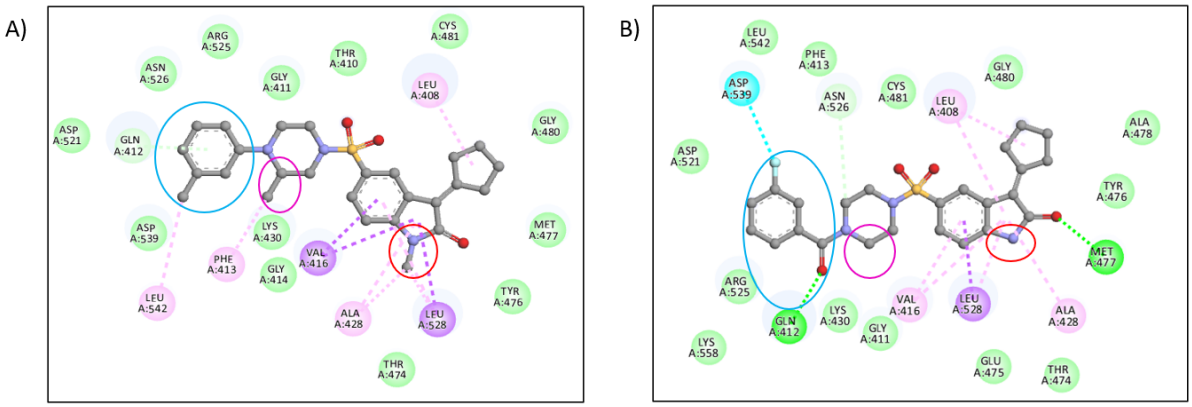

Figure 4. Structure-based pharmacophore modelling of compound **819** (A) to **9g** (B) for better interaction, the blue colour ring shows the replacement of methyl benzyl with 3-fluoro benzoyl, the pink colour ring shows the replacement of methyl group with hydrogen, the red colour ring shows the replacement of methyl group with hydrogen.

In the compound **9b**, the cyclohexane group showed Vander Waal interaction with ASP- 521, ARG-525, ASN-526, TYR-551, LYS-558 amino acids, and Pi-sigma bond with VAL-416, alkyl interactions with LEU-408, LEU-528, ALA-428. The hydrogen bonds are formed with GLN-412 and MET-477 with 2.89 Å, and the free binding energy is -10.8 Kcal/mol. In compound **9f**, the bromine group showed Pi-alkyl interaction with PHE-413, alkyl interaction with LEU-542, and Vander Waal interaction with ASP-539 amino acid. Similarly, hydrogen bonds are formed with GLN-412 with 2.94 Å and MET-477 with 3.18 Å and a free binding energy of -11.1 Kcal/mol. For compound **9g**, the fluorine group forms a Pi-sigma bond with DFG residue ASP-539 in the H3 pocket, an essential amino acid **(Figure 5).** Similarly, the hydrogen bonds are formed with GLN-412 with 2.91 Å and MET-477 with 3.01 Å, and the free binding energy is -11.3 Kcal/mol.

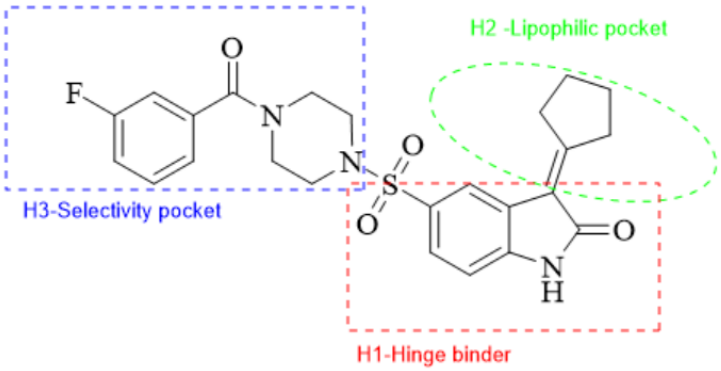

Figure 5. Schematic representation of the interaction of BTK with **9g**.

In compound **9h**, the aliphatic chain showed Vander Waal interaction with only ASP- 521, ARG-525, TYR-551, and LYS-558 amino acids and Pi-sigma bond with VAL-416, alkyl interactions with LEU-408, LEU-528, ALA-428. The hydrogen bonds are formed with GLN-412 with 2.93 Å and MET-477 with 3.21 Å, as shown in **Figure 6**, and the free binding energy is -10.8 Kcal/mol. The crystal structure of BTK complexed with the co-crystal structure with four compounds, **9b, 9f, 9g, and 9h,** is shown in **Figure 7.**

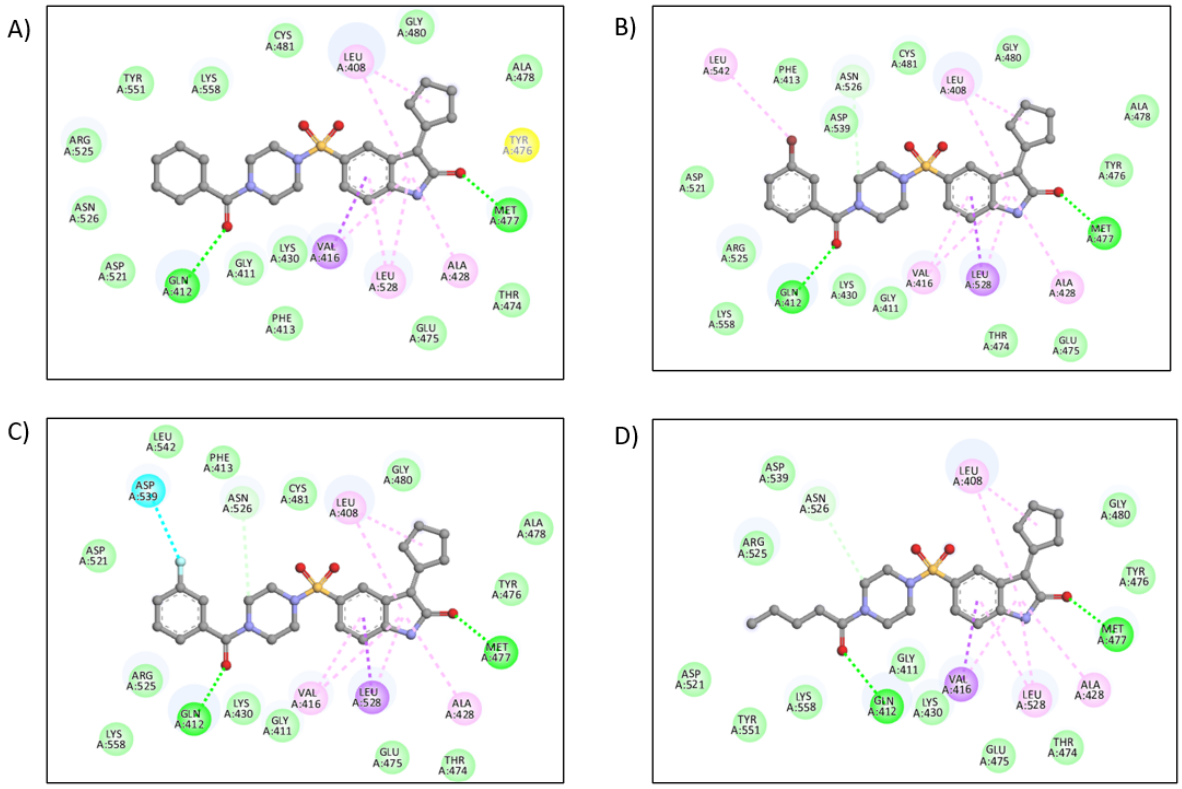

Figure 6. Active site of BTK (PDB-ID-5P9J) showing interactions with compounds (A) **9b**, (B) **9f**, (C) **9g**, (D) **9h** with amino acids GLY-411, ASP-539, MET-477, VAL-416, LYS-430.

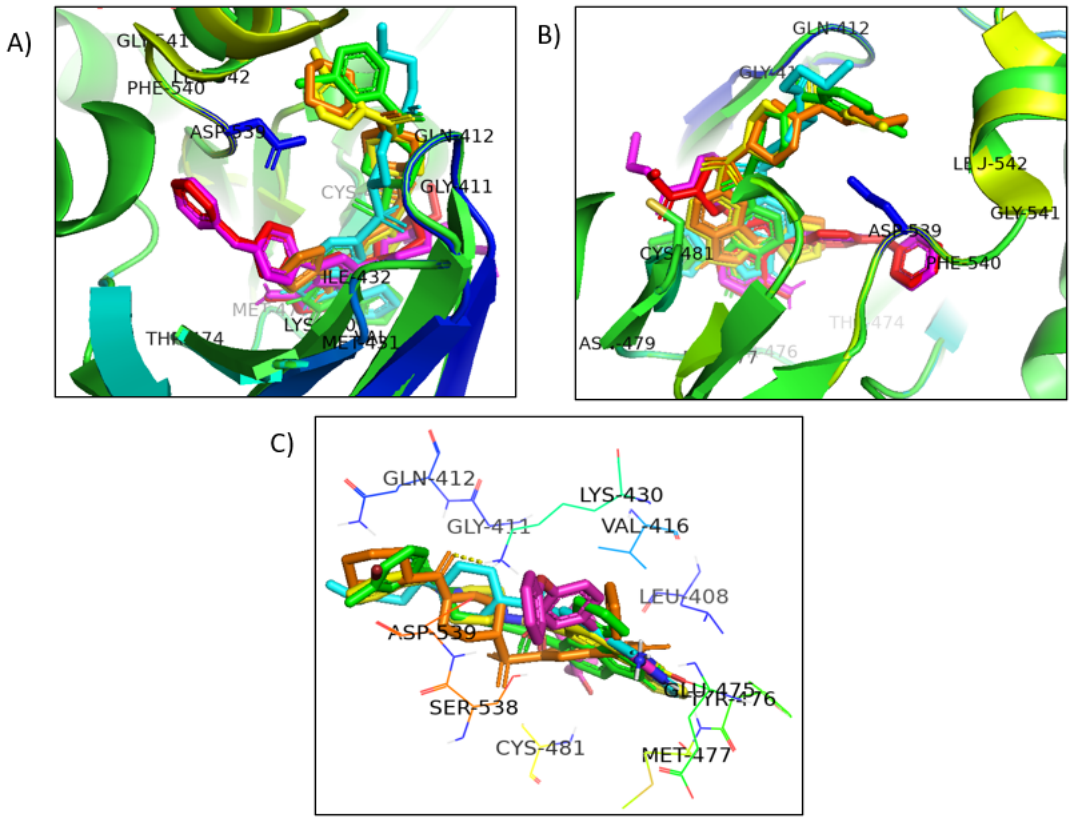

Figure 7. (A) Docking poses of the four compounds **9b**-orange, **9f**-yellow, **9g**-green, **9h**-cyan along with co-crystal structure-pink and redocked co-crystal structure-red at same RMSD. (B, C) Active site images of compounds **9b**-orange, **9f**-yellow, **9g**-green, **9h**-cyan with cocrystal-pink.

Molecular dynamic simulations

MD simulations at 50ns, 20ns, and 20ns were performed for the complex compound 9f-5P9J, 9g-5P9J, and 9h-5P9J. Several factors, such as the ligand protonation state, conformation of ligands, water molecules, cofactors, ions, and conformational and solvation entropies, will affect docking predictions in an unexpected pattern. Many reports support the role of MD simulations in filtering docking results [23,24]. MD simulations were carried out to determine the ligand-protein docked complex's interaction stability. The stereochemical solid geometries of the residues were analyzed for the final structure using the Ramachandran map **(Figure 8).** The residues percentage in the favoured region is 95.69 % (267 residues), the allowed is 3.58 % (10 residues), and the outlier is 0.71 % (2 residues).

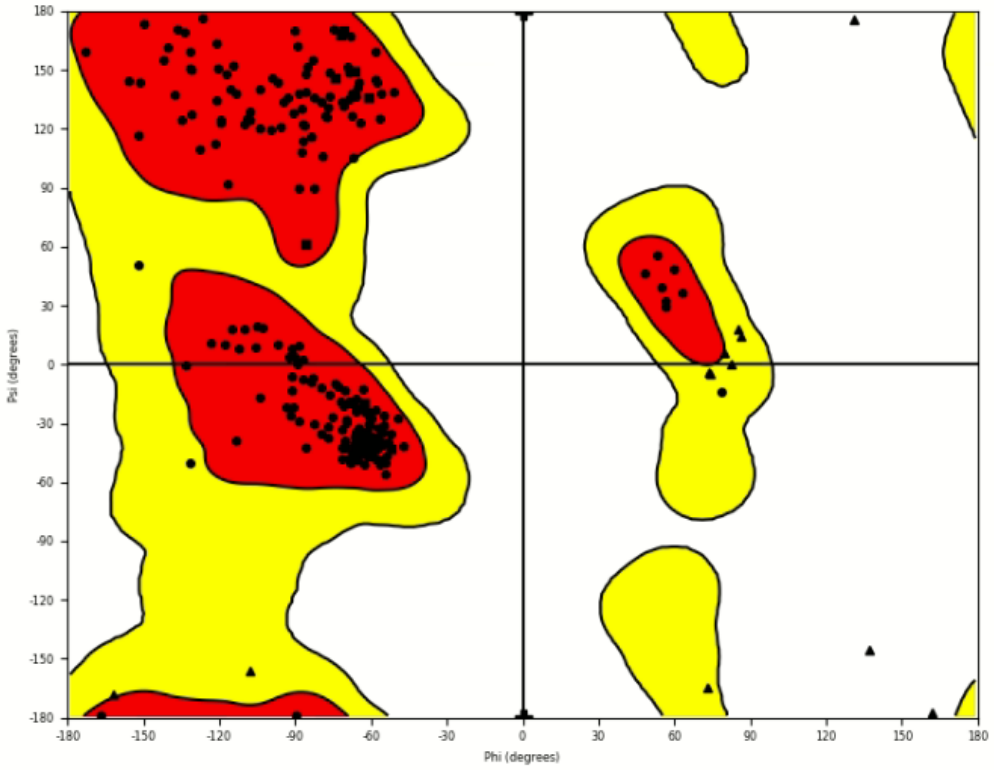

Figure 8. Ramachandran plot depicting stereochemical geometry for compound **9h**-5P9J complex.

The Root Mean Square Deviation (RMSD) of the Cα, backbone, and side chains for all complexes showed fluctuations between the range of 0.4− 3.2 Å, which are in the acceptable range. The results showed that the simulation equilibrated after 4 ns. The RMSD values of Cα and ligand for the complex 5P9J-**9h** were shown in **Figure 9A.** The protein's secondary structure elements (SSE) were monitored during the simulations **(Figure 9B)**. The total percentage of SSE for **9f, 9g,** and **9h** was found to be 42.95 %, 45.71 %, and 44.49 %, respectively. The RMSD values of Cα and ligand, SSE for the complex 5P9J-9f and complex 5P9J-9g were shown in **Figures S1(A), S1(B), S2(A), and S2(B),** respectively. The Protein-RMSF (Root Mean Square Fluctuation) was monitored to analyze the local changes along the protein chain. The ligand-RMSF was examined to study the fluctuations at the atom level, as shown in **Figure 10A**. The brown line indicates "Fit on Protein," and the pink line indicates "Fit on Ligand." The compound 9h interacted with GLY-412 and MET-477, making hydrogen bonds without water. In the presence of water, MET-477 bonded 100 % through simulation, PHE-413 with 65%, and GLY-412 with 36 %. The hydrogen water bonds formed are GLU-475 at 69%, THR-474 at 49%, and CYS-481 at 43%, as shown in **Figure 10B**. The results showed the role water molecules play within the binding pocket of the protein 5P9J for the compound **9h.** The percentage of contacts

between compounds **9f and 9g** with the protein are given in **Figures S3(A), S3(B), S4(A), and S4(B).** Noticeably, both the compounds showed fewer interactions than the compound **9h.** The other interacting residues of the compound **9h** are LEU-408, THR-410, GLY-411, GLU-412, PHE-413, GLY-414, LYS-417, ALA-428, LYS- 430, THR-474, GLU-475, TYR-476, MET-477, CYS-481, ASN-484, ARG-525, ASN-526, CYS-527, LEU-528, VAL-537, ASP-539, VAL-546, TYR-551 as shown in **Figure S5**, where RMSF values are less than 3.6 Å. The green colour indicates the compound **9h**, the maroon colour indicates the B factor, and the orange and the blue bands indicate helices and β-strands, respectively. The B factor and Cα are parallel, indicating the results correlate. In **Figure S6**, the top panel shows the total number of contacts the compound **9h** made throughout the trajectory. In contrast, the bottom panel showed the specific contacts made with the protein throughout the trajectory in each frame. The compound **9h** formed a hydrogen bond with residue MET-477, hydrogen and water bridge interaction with GLN-412, PHE-413, GLU-475, CYS-481, hydrophobic interactions with VAL-416, ALA-428, TYR-476, LEU-528, and water bridge bonds with LEU-408, THR-410, GLY-414, THR-474, ARG-525, as shown in the **Figure S7**. The radial plot gave the details of torsion angle conformation at the simulation time, as shown in **Figure S8.** The 2D diagram of the compound **9h** is presented with colour-coded rotational bonds. The bar plots gave information about the torsion angle's density and the rotational bond's potential in kcal/mol. The torsion potential relationships of the compound **9h** with conformational strain were explained, conserving a protein-bound confirmation. The stability of the ligand was analyzed using six parameters: PSA (polar surface area), RMSD (root mean square deviation), SASA (solvent accessible surface area), MolSA (molecular surface area), IntraHB, rGyr (radius of gyration), shown in **Figure S9**. The RMSD of the ligand was shown to be stable, which ranged up to 1.5 A^0. The histogram graphs, torsional analysis, and stability analysis of the ligands for the compounds **9f** and **9g** were shown in **Figures S10 to S15.**

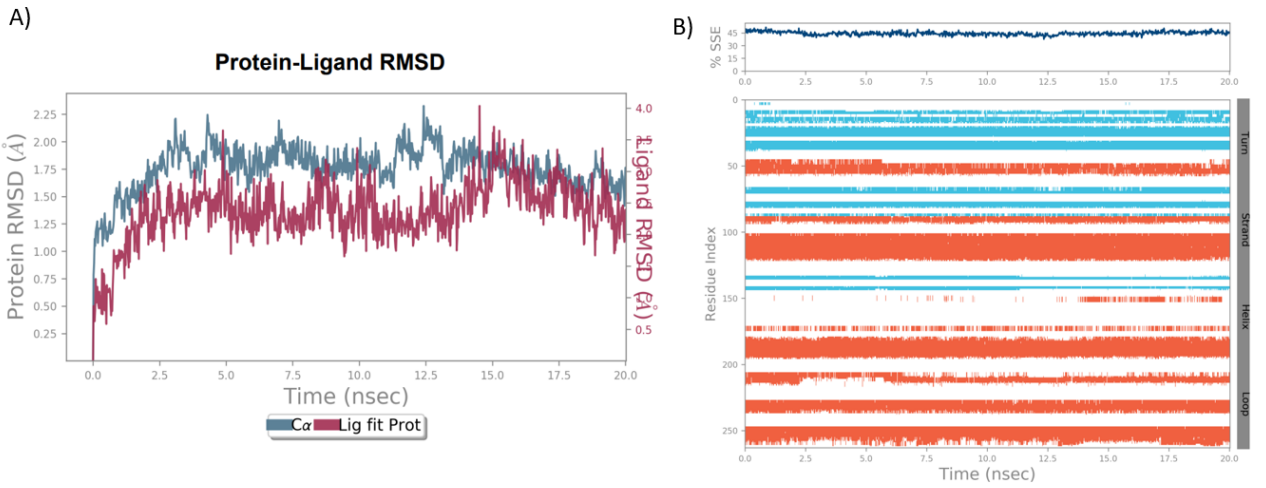

Figure 9. (A) RMSD plot of protein (5P9J) and ligand (**9h**). (B) The secondary structure elements (SSE) of the protein shown with helices in blue colour and beta strands in orange colour.

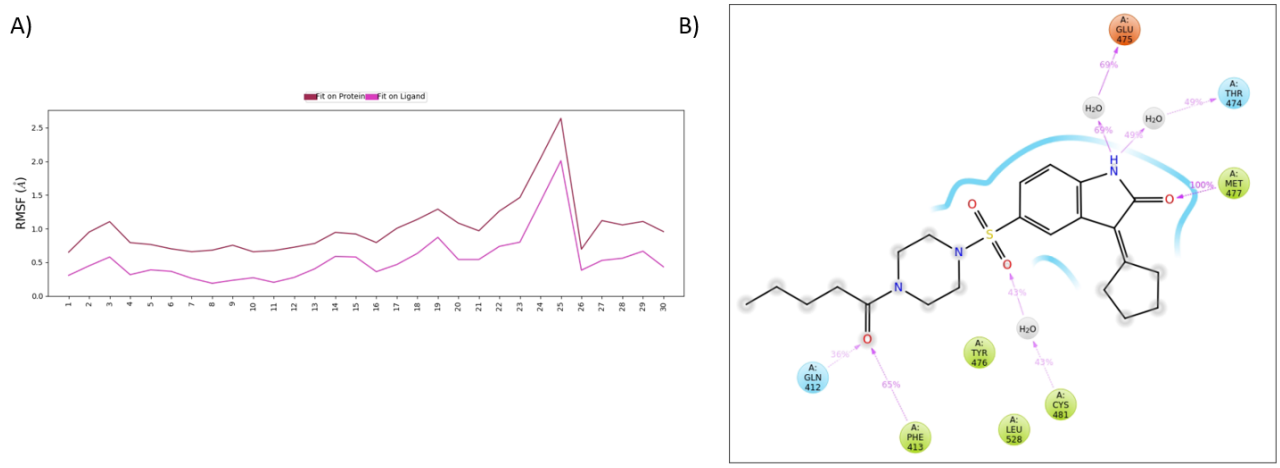

Figure 10. (A) ligand-RMSF plot for compound 9h-protein 5P9J, where the brown line indicates the ligand fluctuations regarding the binding site residues on the target protein and the pink line indicates the fluctuations where the ligand in each frame was aligned on the ligand in the first reference frame. (B) The compound **9h** shows interacting residues.

Synthesis

Commercially available oxindole was used as a starting material for synthesizing 5-substitued Oxindole derivatives. To the chlorosulfonic acid added, oxindole portion wise at 0°C and stirred for 30 mins at room temperature. The mixture was heated to 70°C using an oil bath to afford 2-oxoindoline-5-sulfonyl chloride **2** [25, 26]. The sulfonyl chloride intermediate **2** was coupled in

the presence of pyridine with *N*-Boc piperazine **3** [27, 28], resulting in the *N*-Boc 4-(2-oxoindoline-5-sulfonamido) piperazine **4**. The intermediate **4** in ethanol was subjected to Knoevenagel condensation with cyclopentanone **5** by adding pyrrolidine as a base that affords intermediate **6** [29, 30]. The protecting group tertiary butyl carbonyl of intermediate **6** was removed by treating it with 4M HCl in 1,4-dioxane to yield the critical scaffold **7** as an HCl salt. The analogues **9a-9j** were synthesized by amide coupling with different acid chlorides **8a-8j** in the presence of di isopropyl ethyl amine. The liberated hydrochloric acid was neutralized by added base di isopropyl ethyl amine (**Scheme 1**).

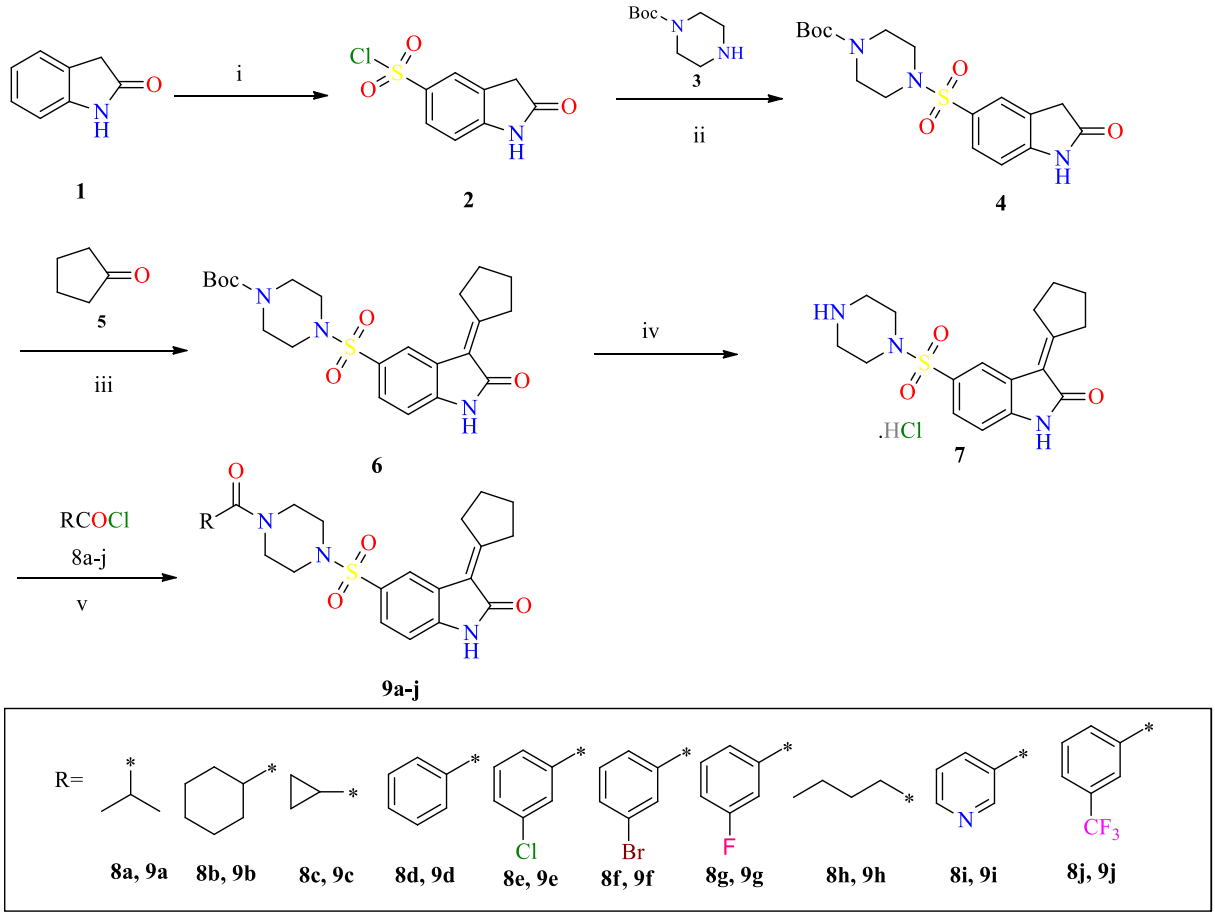

Scheme 1. Synthesis of 5-substituted oxindole derivatives. *Conditions:* (i) $ClSO_3H$, 70 °C, 2 h (ii) Pyridine, 1,4-dioxane, rt, 2 h (iii) Piperazine, EtOH, rt, 2 h, (iv) 4M HCl in 1,4-dioxane, rt, 16 h, (v) DIPEA, CH_2Cl_2, rt, 3 h.

Cytotoxicity of compounds in cell cultures

Ten derivatives were tested in a panel of cell lines consisting of ITK-positive T-cell leukemia lines [31], BTK-positive B-cell leukemia lines [32], ITK/BTK-negative malignant lines, and two non-malignant fibroblast lines. RAMOS and K562 cell lines are BTK-positive with no ITK

expression. RAMOS exhibits higher BTK expression compared to K562 (Data not shown). In contrast, ITK expression is higher in JURKAT than in CCRF-CEM cells, both of which lack BTK expression (Data not shown). RAMOS is well-known for its high BTK expression [32]. Other panel cell lines, including A549, HCT116, U2OS, MRC-5, and BJ, do not express BTK or ITK (Data not shown).

The compounds that did not show 50% inhibition of cell proliferation when evaluated at a single dose of 50 μM were not processed for dose-response analysis. The cytotoxicity profiling was done by considering compounds with IC_{50} values above 50 μM as inactive, above 30 μM as weakly active, between 10 to 20 μM as moderately active, and below 10 μM as highly active. Based on these standard norms, the effects of four structurally similar compounds (active – **9b, 9f, 9g,** and **9h**) were interesting to observe in BTK-high cell lines (**Table 2**). These four compounds were inactive in A549, HCT116, U2OS, JURKAT, and non-malignant cells. Of all the ten compounds, four compounds, **9b, 9f, 9g,** and **9h,** showed activity in RAMOS cells.

The isopropyl group in compound **9a** attached to the piperazine moiety shows no activity. Replacing it with cyclohexyl moiety in compound **9b** showed promising activity in RAMOS cells with IC_{50} of 3.04 ± 0.56 μM. The compounds **9c**, **9d,** and **9e,** having cyclopropyl, benzoyl, and 3-chlorobenzoyl groups attached to piperazine moiety, did not show any activity in RAMOS cells. The compounds **9f** and **9g** having 3-bromobenzoyl and 3-fluorobenzoyl groups to piperazine moiety showed promising activity in RAMOS cells with IC_{50} 2.06 ± 0.43μM, 2.09 ± 0.47 μM, respectively. The compound **9h** with aliphatic group replacement showed promising activity in RAMOS cells with an IC_{50} value of 2.75 ± 0.80 μM. The compounds **9i** and **9j** with pyridine and trifluoro benzoyl moieties attached to piperazine showed no activity in RAMOS cells. The SAR profiling indicates that group cyclopentylidene at the C3 position in compounds **9b, 9f, 9g,** and **9h,** and cyclohexyl in **9b**, 3-bromobenzoyl in **9f,** and 3-fluorobenzoyl in **9g,** valeryl in **9h** attached to carbonyl (C=O) group are essential for biological activity in RAMOS cells **(Table 2).** The compound **9b** showed weak activity in CCRF-CEM cell lines (IC_{50} = 35.53 ± 7.05 μM). Compounds **9g** and **9h** showed weak activity in CCRF-CEM cell lines (**9g**, IC_{50} = 46.46 ± 5.81 μM; **9h**, IC_{50} = 46.15 ± 3.13 μM). Compound **9j** showed moderate activity in U2OS cells (IC_{50} = 23.62 ± 6.44 μM), possibly due to non-specific activity.

We also assessed the cytotoxic effects of ibrutinib, a BTK inhibitor used clinically, on our cell line panel. Compared to the compounds we synthesized, ibrutinib exhibited significant cytotoxic activity against RAMOS cells (IC_{50} = 0.29 ± 0.04), in addition to its activity against BTK-null and ITK-positive cancer cells and non-malignant fibroblast lines (**Table 2**). This is

not surprising given the broad range of kinases inhibited by ibrutinib. However, except for **9j**, none of our synthesized compounds that were effective against BTK-high RAMOS cells displayed any toxicity in both malignant and non-malignant cell lines lacking BTK. This data shows the selective cytotoxicity of our derivates on BTK-high cancer cells.

In vitro pharmacological properties

We next subjected **9b**, **9f,** and **9h** to *in vitro* ADME analyses. Results showed that the three selected are stable in the presence of plasma proteins and bind to proteins with > 85% affinity (**Table 3**). However, **9b** is metabolized quickly by microsomes, suggesting a high probability that the compound will be primarily metabolized in the liver. Compared to **9b**, the intrinsic clearance of **9f** and **9h** was classified as medium in the microsomal stability assay. The passive diffusion mechanism for the three compounds was classified as low to medium by parallel artificial membrane permeability assay (PAMPA). All three compounds showed poor permeability in assays with MDCK-MDR1 cells, indicating a low potential for penetration through the blood−brain barrier. Furthermore, **9b** showed low permeability in Caco-2 cells, suggesting it is unsuitable for oral administration due to poor intestinal absorption. However, the medium permeability of **9f** and **9h** indicate a relatively good human intestinal permeability, suggesting these compounds are suitable for oral administration.

Inhibition of BTK signalling by selected compounds

The effects of **9b**, **9f**, and **9h** at three concentrations were next examined on the activity of BTK Tyrosine 223 phosphorylation [pBTK (Tyr223)]. Although all three compounds decreased pBTK (Tyr223) levels, the decrease was significant following cell treatment with **9h** at 50 µM concentration (**Figure 11A, B**). We next stimulated RAMOS cells with lipopolysaccharide (LPS), a well-known inducer of BTK phosphorylation, which subsequently activates downstream MAPK family proteins, including ERK1/2 and p38 [34]. Additionally, it is established that BTK inhibition blocks the activation of downstream MAPK family proteins [33, 34]. The western protein analysis showed that LPS stimulation significantly activated pBTK (Tyr223) signalling (**Figure 11C, D**). However, pBTK (Tyr223) activation effects were significantly inhibited by **9h**, as evidenced by the decrease in pERK 1/2 (Thr202/Tyr204) and p-p38 (Thr180/Tyr182) levels (**Figure 11D**). These findings, together with cytotoxicity data, suggest that **9h** targets pBTK activities.

Table 2: Biological activity of 10 compounds in ITK/BTK-negative, ITK-positive, and BTK-positive cancer cell lines and non-malignant fibroblast lines. Mean ± SD, n ≥ 6. Representative dose-response curves of **9b**, **9f**, **9g**, **9h** and **9j** are shown in Supplementary Information.

	ITK/BTK-Negative cell lines				ITK-Positive cell lines		BTK-Positive cell lines		Non-cancer	
	A549	HCT116	HCT116 $p53^{-/-}$	U2OS	JURKAT	CCRF-CEM	RAMOS	K562	MRC-5	BJ
9a	>50	>50	>50	>50	>50	>50	>50	>50	>50	>50
9b	>50	>50	>50	>50	>50	35.53±7.05	3.04±0.56	>50	>50	>50
9c	>50	>50	>50	>50	50±0	>50	>50	>50	>50	>50
9d	>50	>50	>50	>50	>50	>50	>50	>50	>50	>50
9e	>50	>50	>50	>50	>50	>50	>50	>50	>50	>50
9f	>50	>50	>50	>50	>50	>50	2.06±0.43	>50	>50	>50
9g	>50	>50	>50	>50	>50	46.46±5.81	2.09±0.47	>50	>50	>50
9h	>50	>50	>50	>50	>50	46.15±3.13	2.75±0.80	>50	>50	>50
9i	>50	>50	>50	>50	>50	>50	>50	>50	>50	>50
9j	>50	>50	>50	23.62±6.44	>50	>50	>50	>50	27.38±6.80	>50
Ibrutinib	-	30±1	30±1	23±3	5±1	4±1	0.3±0	27±3	28±0	29±1

Table 3: Pharmacological properties of **9b**, **9f**, and **9h** determined by *in vitro* and *in vivo* ADME assays.

	Metabolism			Permeability			
	In vitro			*In vitro*		*In vivo*	
	Plasma stability (category)	Microsomal stability (clearance)	Plasma protein binding (% bound)	PAMPA		MDR1-MDCK	Caco-2
				log Pe	*Category*	*CNS (−ive/+ive)*	*Category*
9b	Stable	HIGH	88.60	-6.810	LOW	CNS −ive Papp (x10e-6): 2.92 Efflux ratio: 9.3 Active efflux: Yes % Recovery: 60.23	Low Papp (x10e-6): 3.18 Efflux ratio: 2.69 Active efflux: Yes % Recovery: 45.37
9f	Stable	MEDIUM	95.70	-7.414	LOW	CNS −ive Papp (x10e-6): 3.2 Efflux ratio: 6.93 Active efflux: Yes % Recovery: 79.16	Moderate Papp (x10e-6): 10.59 Efflux ratio: 3.79 Active efflux: Yes % Recovery: 74.54
9h	Stable	MEDIUM	96.66	-5.845	MEDIUM	CNS −ive Papp (x10e-6): 5.43 Efflux ratio: 13.13 Active efflux: Yes % Recovery: 86.9	Moderate Papp (x10e-6): 7.18 Efflux ratio: 3.34 Active efflux: Yes % Recovery: 63.25

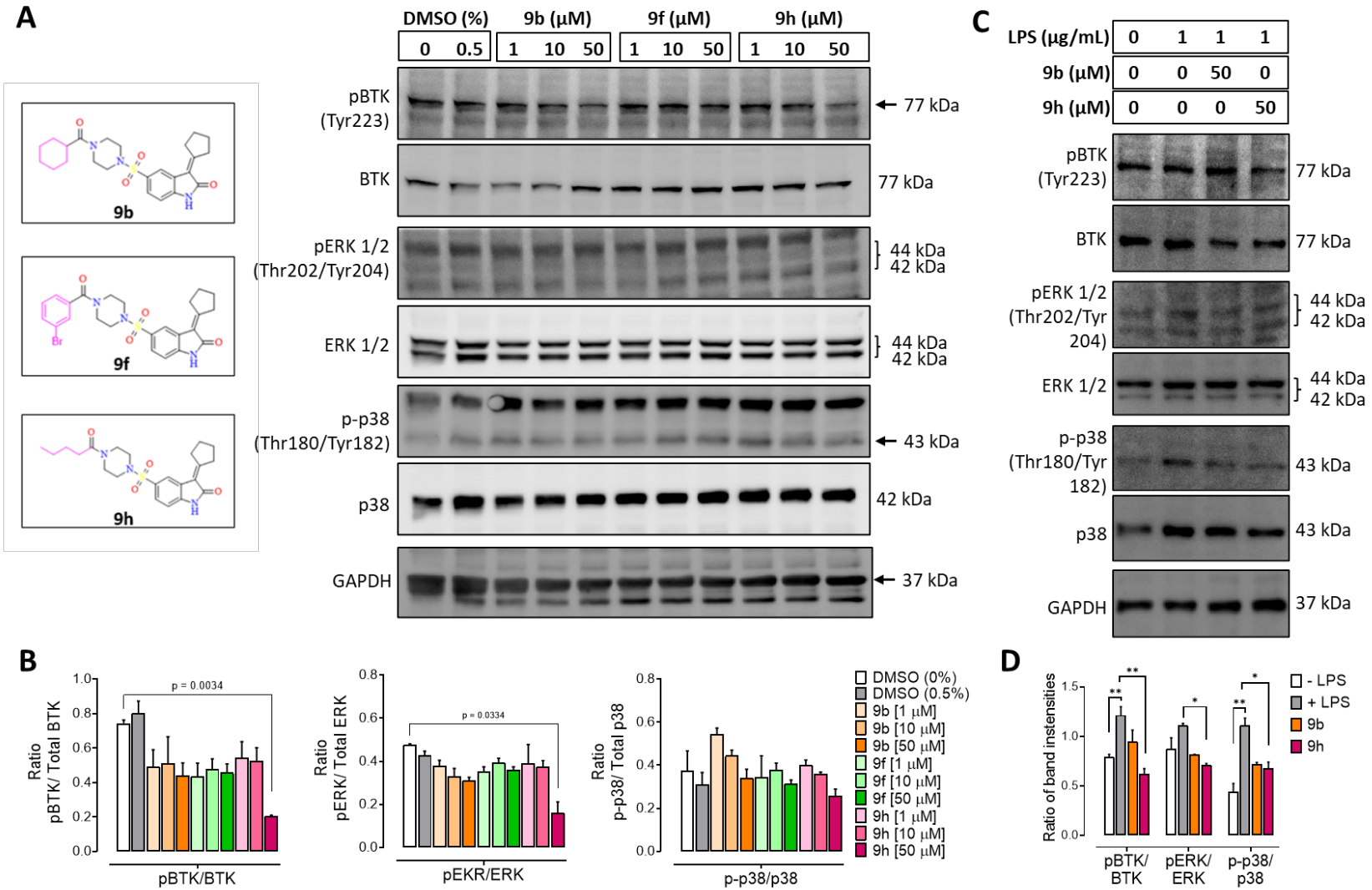

Figure 11. Compound effect on BTK signalling. (A) RAMOS cells were treated with **9b**, **9f**, and **9h** for 24 h at indicated concentrations, and whole protein extracts were probed for phosphorylated and total BTK by Western blotting. (B) Quantification of pBTK/BTK, pERK/ERK and p-p38/p38 band intensities. Mean ± SEM, n = 2-3, One-way ANOVA, Dunnett's multiple comparison test. (C) RAMOS cells were stimulated with LPS for 10 minutes and then treated with **9b** and **9h** at 50 μM concentration for 3 hours, and changes in BTK, ERK1/2, and p38 phosphorylation were probed by Western blotting of whole protein extract. (D) Quantification of pBTK/BTK, pERK/ERK and p-p38/p38 bands shown in panel C. Mean ± SEM, n = 2-3, **P < 0.01, * P < 0.5, One-way ANOVA, Dunnett's multiple comparison test. Images of uncropped blots are shown in Supporting Information.

Conclusion

As initial efforts, we have screened the zinc database using Oxindole as a core moiety to identify new BTK inhibitors. One compound with good binding energy with BTK protein and good ADME properties was chosen to design a focused library. The compound **819** was taken as the lead and further modified for better interactions with the BTK protein, and ten analogous (**9a-9b**) were synthesized. The cytotoxic activity of the compounds was examined in a panel of cancer and non-cancer cell lines. Notably, four molecules, **9b**, **9f**, **9g**, and **9h**, exerted good anticancer activity in the micromole range in BTK-high RAMOS lymphoma cells. Molecular dynamic simulations for compounds **9f**, **9g**, and **9h** were conducted, and the RMSF values were below 2 Å. The RMSD and the ligand-RMSF percentage for Cα indicated the stability of the compounds **9f**, **9g**, and **9h** with 5P9J, and the protein-bound conformations were confirmed by torsional analysis. The compound **9h** showed more protein-ligand contacts in the simulations. All three compounds exhibited low permeability in assays conducted with MDCK-MDR1 cells, indicating limited potential for crossing the blood−brain barrier. Compound **9b** displayed low permeability in Caco-2 cells, suggesting it may not be suitable for oral administration due to poor intestinal absorption. However, the medium permeability observed for **9f** and **9h** in Caco-2 cells suggests that these compounds have relatively good human intestinal permeability, indicating they are suitable for oral administration. The antiproliferative activity of **9h** corresponded to its pBTK (Tyr223) inhibitory activity in RAMOS cells. According to our present findings, **9h** stands out as a promising candidate for further modification and development as a promising inhibitor of BTK-positive cancers.

Materials and Method

Selection of the target molecule

The crystal structure of Bruton's tyrosine kinase (PDB ID: 5P9J, Resolution: 1.08 Å, R-Value Free: 0.224 and R-Value Work: 0.204, No mutations) was obtained from RCSB Protein Data Bank (PDB) [35]. By removing its co-crystallized ligand and water molecules and adding missing residues, the protein was prepared using Swiss PDB Viewer. The SDF files from the ZINC15 database were used as it is for virtual screening. The ligands preparation for the designed molecules were drawn in ChemDraw and saved as SDF files. The schematic representation of the workflow is shown in **Figure 3**.

Structure-based pharmacophore selection

Oxindole was taken as the core moiety to search the molecules from the ZINC15 database, where around 550 molecules were selected and docked with the BTK protein (5P9J) using PyRx Virtual screening tool [36, 37]. The top 19 molecules were selected, considering docking scores above 10 Kcal/mol as criteria. From those 19 molecules, we have designed new molecules based on the pharmacophoric features, which play an essential role in the macromolecule ligand recognition and biological activity shown in **Figure 4.**

Pharmacokinetics and drug-likeness prediction

The compounds finalized after docking using PyRx Virtual screening tool were further proceeded to predict their pharmacokinetics and drug-likeness. The physicochemical properties, pharmacokinetics, Log P, water solubility, and AMES toxicity were predicted by Swiss ADME. The drug-likeness properties were checked with Lipinski violations using Swiss ADME [38, 39] **(Table 1).**

Molecular dynamic simulation

The molecular dynamics (MD) studies were conducted for the complex structures of the 5P9J protein with the selected compound **9f, 9g,** and **9h** using Desmond Software Release 2018-4 for academic licensing (Schrödinger, LLC, New York, NY, USA to check the stability of binding for all the complexes [40]. The simulations used the 0.15 M NaCl and SPC water model to mimic a physiological ionic concentration. Energy minimization was conducted for 100 Pico seconds (ps). The MD simulations were run for 20ns at 300 K and standard pressure (1.01325 bar), with a dimension buffer of 10 Å × 10 Å × 10 Å with an orthorhombic box and an NPT ensemble. The energies were recorded at intervals of 1.2 ps. The MD-simulated net charge system of the protein-

ligand complex was neutralized by adding Na^+ or Cl^- ions. The Nosé-Hoover chain and Martyna-Tobias-Klein algorithms were used to maintain the temperature of all MD systems at 300 K and the pressure at 1.01325 bar.

Chemistry

All the solvents and the reagents used for synthesis were purchased from commercial sources (Sigma Aldrich, Avra, TCI). All reactions were observed by Thin Layer Chromatography using Merck classic aluminium silica plates with a thickness of 200 µm, size 20 x 20 cm, and were checked in Ultraviolet-Visible spectroscopy at 254 nm. All compounds were purified using column chromatography with silica gel (60-100#) as the stationary phase. Proton ^1H and ^{13}C NMR spectra were recorded on an SA-AGILENT 400MHz NMR and (Ascend) AVANCE NEO 600 MHz FT-NMR spectrometer. Proton NMR chemical shifts are reported using tetramethylsilane (TMS) as a standard reference in parts per million (δ). ESI spectra were recorded on Micro mass, Quattro LC using ESI+ software with a capillary voltage of 3.98 kV and ESI mode positive ion trap detector. IR spectra were recorded on an FT-IR spectrometer (Shimadzu FT-IR 8300 spectrophotometer), and peaks were reported in cm^{-1}. Melting points were measured in degrees centigrade (°C) using a melting point apparatus and reported.

2.1 Synthesis of 2-oxoindoline-5-sulfonyl chloride **2**: To ice-cooled chlorosulfonic acid (20 mL), added indolin-2-one **1**(5.0 g, 37.5 mmol) portionwise at 0 °C, stirred at room temperature (RT) for 30 minutes and heated at 70 °C for 1 hr. To the ice-cold water, the reaction mixture was added slowly dropwise after cooling to room temperature and stirred for 30 minutes. The precipitated solid was washed with water (20 mL) thrice. Under reduced pressure, the resulting solid was dried to produce compound 2-oxoindoline-5-sulfonyl chloride **2**. (6.20 g, 71.4%) as light brown solid: ^1H NMR (300 MHz, DMSO–d_6): δ 10.55 (s, 1H), 7.49-7.46 (m, 2H), 6.79 (d, J = 7.8 Hz, 1H), 3.49 (s, 2H); MS (ESI+APCI): m/z = 231.9 $[M + H]^+$.

2.2 Synthesis of *tert*-butyl 4-((2-oxoindolin-5-yl) sulfonyl) piperazine-1-carboxylate (**4**): The 2-oxoindoline-5-sulfonyl chloride **2** (3.00 g, 12.94 mmol) was taken in 1, 4-dioxane (20 mL), added *tert*-butyl piperazine-1-carboxylate **3** (3.60 g, 19.35 mmol), and was charged with pyridine (1.80 g, 25.8 mmol) resultant reaction mixture stirred at room temperature for 2 h. Water (30 mL) was added to the reaction mixture to dilute it. The reaction mixture was then acidified to a pH of 6 with 2N HCl solution and extracted with ethyl acetate (3 50 mL of EtOAc). The mixed organic layer was concentrated under reduced pressure, filtered, and dried over anhydrous Na2SO4. Hexane (2 × 20 mL) washes were given and dried under reduced

pressure to afford *tert*-butyl 4-((2-oxoindolin-5-yl) sulfonyl) piperazine-1-carboxylate (**4**) (3.80 g, 76.9%) as light brown solid (crude directly used for next step without any purification); MS (ESI+APCI): m/z = 380.5 $[M -H]^+$.

2.3 Synthesis of *tert*-butyl 4-((3-cyclopentylidene-2-oxoindolin-5-yl) sulfonyl)piperazine-1-carboxylate (**6**): A solution of *tert*-butyl 4-((2-oxoindolin-5-yl)sulfonyl)piperazine-1-carboxylate 4 (2.8 g, 7.34mmol), cyclopentanone 5 (1.85 g, 22.04 mmol), in EtOH (20 mL) was charged with piperazine (1.87 g, 22.02 mmol), resultant reaction mixture stirred at room temperature for 1 h then heated at 50 °C for 2 h. The reaction mixture was cooled to room temperature, filtered the solid and washed with hexanes (50 mL) to afford compound **6** (1.4 g, 42%) as an off-white solid; 1H-NMR (400 MHz, DMSO-d_6): 10.97 (s, 1H), 7.65-7.56 (m, 2H), 7.06 (d, J = 8.00 Hz, 1H), 3.41-3.38 (m, 4H), 3.02 (t, J = 5.60 Hz, 2H), 2.89 (t, J = 6.00 Hz, 2H), 2.80-2.80 (m, 4H), 1.85-1.75 (m, 4H), 1.34 (s, 9H); MS(ESI+APCI): m/z = 448 $[M + H]^+$.

2.4 Synthesis of 3-cyclopentylidene-5-(piperazin-1-ylsulfonyl) indolin-2-one. HCl (**7**): A solution of compound **6** (1.4 g, 3.13 mmol), in CH_2Cl_2 (10 mL), was added 4M HCl in 1,4-dioxane (10 mL), resulting reaction mixture stirred at room temperature for 16 h. The reaction mixture was concentrated under reduced pressure, solid washed with MTBE (20 mL), and dried to afford 3-cyclopentylidene-5-(piperazin-1-ylsulfonyl)indolin-2-one.HCl (**7**) (1.1 g, 92%) as off-white solid; ^{1}H NMR (400 MHz, DMSO–d_6): δ 11.02 (s, 1H), 9.02 (s, 2H), 7.63-7.61 (m, 2H), 6.10 (d, J = 8.8 Hz, 1H), 3.16-3.13 (m, 8H), 3.03 (t, J = 5.8 Hz, 2H), 2.91 (t, J = 5.8 Hz, 2H), 1.89-1.74 (m, 4H); MS (ESI+APCI): m/z = 348 [M + H] +.

2.5 General procedure for the synthesis of 8: To a solution of compound 7 (1.0 equiv.) in CH_2Cl_2 (3.0 mL) was added DIPEA (3.0 equiv.) followed by RCOCl (1.2 equiv.) at room temperature. The resultant reaction stirred at rt for 3 h. The reaction mass was quenched with water and extracted with EtOAc (5 mL). The organic layer dried over Na_2SO_4 and concentrated under reduced pressure to afford compound 9. All series of compounds **9a-j** were synthesized using the same procedure.

2.5.1.1: 3-cyclopentylidene-5-((4-isobutyrylpiperazin-1-yl) sulfonyl) indolin-2-one (compound **9a**): The compound **9a** was obtained from the 3-cyclopentylidene-5-(piperazin-1-ylsulfonyl)indolin-2-one hydrochloride (**7**) and isobutyryl chloride **8a** as off white solid; yield 72.8%; Melting point (MP): 165-171°C; IR (KBr): υ (cm^{-1}): 1622 (-C=O for amide),1702 (-C=O for amide), 3543 (-NH for secondary amine), 1325 (-SO_2 bending for methylene), 1452 (-c=c- for aromatic); ^{1}H-NMR (400 MHz, DMSO–d_6): δ 10.93 (s, 1H, -NH), 7.59-7.56 (m, 2H, Ar-H), 7.06-7.03 (d, J = 12 Hz, 1H, Ar-H), 3.58-3.53 (m, 4H, -CH_2-CH_2-), 3.04-2.99 (m, 2H, -NCH_2- piperazine), 2.89-

2.86 (m, 6H, -NCH$_2$- piperazine), 2.77-2.75 (m, 1H, -CH- isobutyl), 1.87-1.75 (m, 4H, -CH$_2$-CH$_2$- cyclopentylidene), 0.91(d, J = 6.4 Hz, 6H,-C(CH$_3$)$_2$- isobutyl); ^{13}C NMR (600 MHz, CDCl$_3$): δ 26.15, 26.94 (-***C***H$_2$(C=C), 32.89, 35.44 (-***C***H$_2$-*C*H$_2$), 13.81, 22.69, 25.77, 27.19 (-***C***H$_2$, Aliphatic), 40.83, 41.97, 45.98, 46.20 (-N(***C***H2) piperazine), 109.49, 118.61, 121.89, 124.87, 127.73, 127.90, 143.60 (Ar-***C***), 168.96 (-CH=***C***H), 170.50 (-N(*C*=O), 171.70 (-***C***=O(NH)); MS (ESI+APCI): m/z = 418.34 [M + H]$^+$

2.5.1.2: 5-((4-(cyclohexanecarbonyl) piperazin-1-yl) sulfonyl)-3-cyclopentylideneindolin-2-one (compound **9b)**: The compound **9b** was obtained from 3-cyclopentylidene-5-(piperazin-1-ylsulfonyl) indolin-2-one hydrochloride (**7**) and cyclohexanoyl chloride **8b** as a light brown solid. Melting point (MP): 140-145°C -, Yield: 84.61%. FT- IR (KBr): *v*cm−1:1620 (-C=O for amide):; 1710cm−1(-C=O for amide):; 3423 (-NH for secondary amine); 1346 (-so$_2$ bending for methylene); 1462 (-c=c- for aromatic); ^{1}H-NMR (400MHz, DMSO–d_6), δ 10.95 (1s, 1H, -NH), 7.72-7.81 (d, 2H, Ar-H), 7.06 (s, 1H, Ar-H), 3.54-3.35 (m, 4H, piperazine), 3.01-2.87 (m, 6H), 1.87-1.65 (m, 7H, cyclopentylidene), 1.41-0.91 (m, 10H, cyclohexane); ^{13}C NMR (600MHz, CDCl$_3$) δ 25.68, 26.18 (***C***H2(C=C), 35.47, 36.07 (***C***H2(CH2)), 20.70, 22.66, 29.06, 31.59, 34.66, 40.83 (CH2, Cyclic), 42.71, 44.77, 46.04, 46.41 (N(***C***H2)), 109.43, 118.52, 121.95, 124.89, 127.72, 128.05, 143.36 (Ar***C***),168.88 (CH=***C***H), 170.71 (N(*C*=O), 174.64 (-***C***=O(NH)); MS (ESI+APCI): m/z = 458.20[M + H]$^+$

2.5.1.3: 3-cyclopentylidene-5-((4-(cyclopropane carbonyl) piperazin-1-yl) sulfonyl) indolin-2-one (compound **9c)**: The compound **9c** was obtained from 3-cyclopentylidene-5-(piperazin-1-ylsulfonyl)indolin-2-one hydrochloride (**7**) and cyclopropanoyl chloride **8c** as a light brown solid. Melting point (MP): 136-142°C, Yield : 90.30%; FT- IR (KBr): *v*cm−1 :1637 (-C=O for amide); 1704 (-C=O for amide); 3408 (-NH for secondary amine); 1338 (-so$_2$ bending for methylene); 1453 (-c=c- for aromatic);^{1}H-NMR (400MHz, DMSO–d_6), δ 10.94 (s, 1H, -NH), 7.60-7.56 (m, 2H, Ar-H), 7.05 (d, J = 8.0 Hz, 1H, Ar-H), 3.74-3.54 (m, 4H), 3.01-2.99 (m, 2H, piperazine), 2.91-2.88 (m, 6H), 1.89-1.75 (m, 5H, cyclopentylidene), 0.65-0.63 (m, 4H, cyclopropyl); ^{13}CNMR (400MHz, CDCl$_3$) δ7.73 (***C***H2(CH2)), 10.88 (***C***H(C=O)), 25.78, 26.15 (***C***H2(C=C), 35.00, 35.44, ((***C***H2(CH2)), 45.71, 45.90, 45.94, 46.01 ((***C***H2(NH)), 109.29, 118.49, 121.98, 124.94, 127.75, 128.0, 143.36 (Ar-***C***), 168.55 (-CH=***C***H), 170.44 (-N(*C*=O), 172.05 (-***C***=O(NH)); MS(ESI+APCI):m/z = 416.17[M + H]$^+$

2.5.1.4: 5-((4-benzoylpiperazin-1-yl) sulfonyl)-3-cyclopentylideneindolin-2-one (compound **9d)**: The compound **9d** was obtained from 3-cyclopentylidene-5-(piperazin-1-ylsulfonyl)

indolin-2-one hydrochloride (**7**) and benzoyl chloride **8d** as a light brown solid. Melting point (MP): 135-140°C, Yield : 80.07%; FT- IR (KBr): *v*cm−1: 1617 (-C=O for amide) ; 1708 (-C=O for amide); 3418 (-NH for secondary amine) ; 1344 (-SO_2 bending for methylene);1455 (-c=c- for aromatic);^{1}H-NMR (400MHz, DMSO–d_6), δ 10.94 (s,1H, -NH), 7.94 (d, *J* = 8.00Hz, 1H, Ar-H), 7.60-7.33 (m, 6H, Ar-H) 7.05 (d, *J* = 8.0 Hz, 1H, Ar-H), 3.64 (m, 4H, cyclopentylidene), 3.01-2.66 (m, 8H, piperazine), 1.77-1.84 (m, 4H, cyclopentylidene); ^{13}C NMR (600 MHz, CDCl3) δ 25.77, 26.14 (***C***H2(C=C), 35.09, 35.53 (***C***H2(CH2)), 46.01, 46.14, 46.18, 46.35 (-N(***C***H2)), 109.53, 118.52, 121.97, 127.15, 127.73, 128.14, 127.73 130.13, 130.26, 133.58, 134.72, 143.33 (Ar-***C***), 169.09 (-CH=***C***H), 170.11 (-N(*C*=O), 171.06 (-***C***=O(NH)); MS (ESI+APCI): m/z = 452.16$[M + H]^+$

2.5.1.5: 5-((4-(3-chlorobenzoyl) piperazin-1-yl) sulfonyl)-3-cyclopentylideneindolin-2-one (compound **9e)**: The compound **9e** was obtained from 3-cyclopentylidene-5-(piperazin-1-ylsulfonyl) indolin-2-one hydrochloride (**7**) and 3 chlorobenzoyl chloride **8e** as a light brown solid. Melting point (MP): 133-138°C, Yield: 87%; FT- IR (KBr): *v*cm−1: 1615 (-C=O for amide); 1708 (-C=O for amide); 3445 (-NH for secondary amine); 1285 (-SO_2 bending for methylene); 1442 (-c=c- for aromatic) ; ^{1}H-NMR (400 MHz, DMSO–d_6): δ 10.94 (s, 1H, -NH), 7.60-7.50 (m, 2H, Ar-H), 7.49-7.48 (m, 1H, Ar-H), 7.44-7.43(m, 1H, Ar-H), 7.43-7.39 (m, 2H, Ar-H), 7.05 (d, *J* = 8.00 Hz, 1H, Ar-H), 3.70-3.66 (m, 2H, cyclopentylidene), 3.41-3.38 (d, *J* = 12.00 Hz, 2H, cyclopentylidene), 3.03-2.87 (m, 8H, piperazine), 1.86-1.75 (m, 4H, cyclopentylidene)); MS (ESI+APCI): m/z = 486.28$[M + H]^+$

2.5.1.6: 5-((4-(3-bromobenzoyl) piperazin-1-yl) sulfonyl)-3-cyclopentylideneindolin-2-one (compound **9f**): The compound **9f** was obtained from 3-cyclopentylidene-5-(piperazin-1-ylsulfonyl) indolin-2-one hydrochloride (**7**) and 3 bromobenzoyl chloride **8f** as a light brown solid. Melting point (MP): 130-135°C, Yield : 76.51%; FT- IR (KBr): *v*cm−1:1615 (-C=O for amide); 1701 (-C=O for amide); 3447 (-NH for secondary amine); 1309 (-SO_2 bending for methylene); 1435 (-c=c- for aromatic); ^{1}H-NMR (400 MHz, DMSO–d_6): δ 10.9 (s, 1H, -NH), 7.84-7.82 (m, 1H, Ar-H), 7.64-7.55 (m, 2H, Ar-H), 7.48 (d, *J* =8.00 Hz, 1H, Ar-H), 7.38-7.33 (m, 2H, Ar-H), 7.06 (d, *J* = 12.00 Hz, 1H, Ar-H), 3.64 (d, *J* = 32.00 Hz, 4H, cyclopentylidene), 3.03-2.87 (m, 8H, piperazine), 1.86-1.75 (m, 4H, cyclopentylidene); ^{13}C NMR (600 MHz, $CDCl_3$) δ 25.76, 26.13 (***C***H2(C=C), 35.15, 35.58(***C***H2(CH2)), 45.91(-N(***C***H2)), 109.75, 118.56, 121.93, 122.81, 124.89, 125.60, 127.75, 128.65, 130.24, 131.72, 133.31, 136.65, 143.35 (Ar-***C***), 168.76 (-CH=***C***H), 169.58 (N(*C*=O), 71.56 (-***C***=O(NH)); MS (ESI+APCI):m/z = 532.22$[M + H]^+$

2.5.1.7: 3-cyclopentylidene-5-((4-(3-fluorobenzoyl) piperazin-1-yl) sulfonyl) indolin-2-one (compound **9g**): The compound **9g** was obtained from 3-cyclopentylidene-5-(piperazin-1-ylsulfonyl) indolin-2-one hydrochloride (**7**) and 3 fluorobenzoyl chloride **8g** as a cream colour solid. Melting point (MP): 132-135°C, Yield : 78%; FT- IR (KBr): *v*cm−1; 1624 (-C=O for amide); 1704 (-C=O for amide); 3448 (-NH for secondary amine); 1335 (-SO_2 bending for methylene): cm−1; 1449 (-c=c- for aromatic); ^{1}H-NMR (400 MHz, DMSO–d_6): δ 10.97 (s, 1H, -NH), 7.60-7.56 (d, *J* = 16.00 Hz, 2H, Ar-H), 7.46-7.44 (d, *J* = 8.0 Hz, 1H, Ar-H), 7.27-7.16 (m, 3H, Ar-H), 7.07-7.05 (d, *J* = 8 Hz,1H, Ar-H l), 3.99-3.03 (m, 4H), 3.69 (m, 3H), 3.37 (s, 1H, piperazine), 2.91-2.80 (m, 4H), 1.86-1.75 (m, 4H, cyclopentylidene); ^{13}C NMR (400 MHz, $CDCl_3$) δ 25.76, 26.17 (***C***H2(C=C), 35.05, 35.48 (***C***H2(CH2)), 46.05 (N(***C***H2)), 109.57, 114.33, 114.56, 117.19, 118.59, 121.91, 122.77, 124.95, 127.95, 130.57, 136.81, 143.59, 161.28 (Ar-***C***), 163.75(-CH=***C***H), 168.97 (-N(*C*=O), 170.77 (-***C***=O(NH)); MS (ESI+APCI): m/z = 470.12 $[M + H]^+$

2.5.1.8: 3-cyclopentylidene-5-((4-pentanoyl piperazin-1-yl) sulfonyl) Indolin-2-one (compound **9h)**: The compound **9h** was obtained from 3-cyclopentylidene-5-(piperazin-1-ylsulfonyl) indolin-2-one hydrochloride (**7**) and valeroyl chloride (**8h**) as an off-white solid. Melting point (MP): 130-135°C, Yield : 76.51%; FT- IR (KBr): *v*cm−1; 1632 (-C=O for amide) ; 1701 (-C=O for amide); 3405 (-NH for secondary amine); 1326 (-SO_2 bending for methylene); 1452 (-c=c- for aromatic); ^{1}H-NMR (400 MHz, DMSO–d_6): δ 10.94 (s, 1H, -NH), 7.59-7.55 (m, 2H, Ar-H), 7.05 (d, *J* = 12.00 Hz, 1H, phenyl), 3.51 (s, 4H), 3.02 (d, J = 8.00 Hz, 2H), 2.99-2.83 (m,6H), 2.24-2.20 (m,3H), 1.87-1.83 (m,4H), 1.78-1.75 (m, 3H), 1.39-1.33 (m,6H), 1.25-1.20 (m, 3H, aliphatic, valeroyl); ^{13}CNMR (600MHz, CDCl3) δ 26.15, 26.94 (***C***H2(C=C), 32.89, 35.44 (***C***H2(CH2)), 13.81, 22.69, 25.77, 27.19 (CH2,Aliphatic), 40.83, 41.97, 45.98, 46.20(-N(***C***H2)), 109.49, 118.61, 121.89, 124.87, 127.73, 127.90, 143.60 (Ar-***C***), 168.96 (-CH=***C***H), 170.50 (-N(*C*=O), 171.70 (-***C***=O(NH)); MS (ESI+APCI): m/z = 432.14 $[M + H]^+$

2.5.1.9: 3-cyclopentylidene-5-((4-nicotinoylpiperazin-1-yl) sulfonyl) indolin-2-one (compound **9i):** The compound **9i** was obtained from 3-cyclopentylidene-5-(piperazin-1-ylsulfonyl) indolin-2-one hydrochloride (**7**) and 3-pyridine chloride **8i** as an off-white solid. Melting point (MP): 195-200°C, Yield : 62%; FT- IR (KBr): *v*cm−1; 1610 (-C=O for amide); 1704 (-C=O for amide); 3414 (-NH for secondary amine); 1332 (-SO_2 bending for methylene); 1464 (-c=c- for aromatic); ^{1}H-NMR (400 MHz, DMSO–d_6): δ 10.94 (s, 1H, -NH), 8.62 (d, *J* = 4.00 Hz, 1H, Ar-H), 8.52 (d, J = 8.00 Hz, 1H), 7.78 (d, *J* = 12.00 Hz, 1H, Ar-H), 7.60-7.56 (m, 2H), 7.44-7.41 (m, 1H), 7.06 (d, *J* =12.00 Hz, 1H, Ar-H), 3.71-0.00 (m, 2H), 3.41-3.37 (m, 2H, cyclopentylidene), 3.03-2.87 (m, 8H,

piperazine), 1.86-1.75 (m, 4H, cyclopentylidene); ^{13}C NMR (600 MHz, $CDCl_3$) δ 25.17, 26.13 (***C***H2(C=C), 35.04, 35.48(***C***H2(CH2)), 45.89, 46.02, 46.13, 46.68 (-N(***C***H2)), 109.29, 121.98, 123.66, 125.08, 127.72, 127.88, 130.69, 135.25, 143.35, 147.90, 151.26 (Ar-***C***), 167.81 (-CH=***C***H), 168.24 (-N(*C*=O), 170.68 (-***C***=O(NH)): MS (ESI+APCI): m/z = 453.14 $[M + H]^+$

2.5.2.10: 3-cyclopentylidene-5-((4-(3-(trifluoromethyl) benzoyl) piperazin-1-yl) sulfonyl) indolin-2-one (compound **9j)**: The compound **9j** was obtained from 3-cyclopentylidene-5-(piperazin-1-ylsulfonyl) indolin-2-one hydrochloride (**7**) and 3- trifluoromethyl benzoyl chloride **8j** as a light cream solid. Melting point (MP): 139-143°C, Yield: 83%; FT- IR (KBr): *v*cm−1; 1618 (-C=O for amide); 1707 (-C=O for amide); 3445 (-NH for secondary amine): cm−1; 1332 (-SO_2 bending for methylene); 1469 (-c=c- for aromatic);^{1}H-NMR (400 MHz, DMSO–d_6): δ 10.94 (s, 1H, -NH), 7.79-7.56 (m, 7H, Ar-H), 3.40 (d, *J* = 8.00 Hz, 2H), 3.72 (d, J=8.00Hz, 2H, cyclopentylidene), 3.03-2.87 (m, 8H, piperazine), 1.85-1.7 (m,4H, cyclopentylidene); ^{13}CNMR (400MHz, $CDCl_3$): δ 25.76, 26.13 (***C***H2(C=C), 35.12, 35.55 (***C***H2(CH2)), 46.06 (N(***C***H2)), 109.71, 118.58, 121.91, 127.02, 128.15, 129.28, 129.78, 130.40, 131.03, 135.54, 143.47(Ar-***C***), 168.87(-CH=***C***H), 169.45 (-N(*C*=O), 171.35 (-***C***=O(NH)); MS (ESI+APCI): m/z = 520.14 $[M + H]^+$

Cell lines

All cell lines were purchased from ATCC (Middlesex, UK) or DSMZ (Braunschweig, Germany) and maintained according to recommendations at 37°C in a humidified incubator (5% CO2/atmospheric air). Multidrug-resistant sublines (CEM-DNR and K562-TAX) expressing the LRP, and P-glycoprotein transporter proteins were derived and cultured as previously described [41]. Cell lines were routinely tested for mycoplasma contamination and authenticated biweekly or monthly.

Cytotoxicity assay

The cytotoxicity activity of all 10 compounds was tested under *in vitro* conditions using a 3-day standard 3-(4,5-dimethylthiazol-2yl)-5-(3-carboxymethoxyphenyl)-2-(4-sulfophenyl)-2H-tetrazolium reduction assay in 384-well plates on a robotic high-throughput screening platform (HighResBio, Boston, MA) as described elsewhere [41]. The IC_{50} values were calculated from the respective dose−response curves of compounds with Dotmatics (San Diego, CA, USA).

In vitro pharmacology

Selected compounds were assayed for human plasma and liver microsomal stability *in vitro*, a parallel artificial membrane permeability assay (PAMPA) and cellular permeability models of gastrointestinal resorption and the blood-brain barrier using Caco-2 and MDR1-MCDK cells as previously described [41]. Samples were analyzed in an Agilent RapidFire 300 High-Throughput Mass Spectrometry System (RF-MS; Agilent, Wakefield, MA) with subsequent detection in a Qtrap 5500 mass spectrometer (AB Sciex, Concord, Canada).

Western blotting

RAMOS cells were plated at 0.5 x 106/mL density in 6-well plates. After 24 h, cells were treated with compounds at concentrations of 1, 10, and 50 µM for 24 h. The concentration of the vehicle was 0.5% in the highest test drug concentration (50 µM). For LPS stimulation, RAMOS cells in growth media containing 1% FCS were exposed to 1 µg/ml LPS from *Escherichia coli* (O111:B4) (Sigma-Aldrich, Missouri, USA; Cat. # L2630) for 10 minutes. Cells were next centrifuged to remove LPS-containing media and washed twice with complete growth media containing 10% FCS. Stimulated cells were next plated at a density of 0.5 x 10^6/mL in 6-well plates, followed by treatment with compounds for 3 hours.

To obtain whole-cell protein extracts, cells were collected, washed with 1× Tris-buffered saline (TBS), and lysed in RIPA buffer (Thermo Fisher Scientific, Massachusetts, USA), Cat #89901) supplemented with protease (Roche, Basel, Switzerland, Cat. #04693116001) and phosphatase (Roche, Basel, Switzerland; Cat. #04906837001) inhibitors by sonication using a Cup Horn sonicator (Qsonica, LLC., Connecticut, USA). The cell lysate was then centrifuged at 12 000 RPM for 30 min at 4 °C, and the supernatant was collected. Thirty-five µg protein samples were processed for electrophoresis and Western blotting, as described elsewhere [41]. Primary antibodies used were anti-rabbit Btk (1:1000, overnight, 4 °C; Cell Signaling Technology, Inc., Massachusetts, USA; Cat. #3533S), Phosphor-BTK (Tyr223) (1:1000; Cat # 5082S), p44/42 MAPK (ERK1/2) (1:1000; Cat # 9102S), Phospho-p44/42 MAPK (ERK1/2) (Thr202/Tyr204) (1:1000; Cat # 4376S), p38 MAPK (1:1000; Cat # 9212S), Phospho-p38 MAPK (Thr180/Tyr182) (1:1000; Cat # 9211S), and anti-rabbit GAPDH (1:4000, 1 hour, room temperature; Cell Signaling Technology, Inc., Massachusetts, USA; Cat. #2118). Primary antibody-stained blots were developed using anti-mouse (Cat. # A11034) or anti-rabbit (Cat. #A21202) Alexa Fluor 488-conjugated secondary antibodies (Invitrogen, Massachusetts, USA) at 1:2000 dilution for 1–2 h at room temperature in the dark. The blots were then imaged using a Gel Doc XR + Gel Documentation System (Bio-Rad, California, USA) with appropriate

filters for Alexa Fluor 488 to visualize protein bands. Band intensities were quantified using NIH ImageJ Software (NIH, Bethesda, Maryland, USA).

Statistical analysis

All blots were analyzed using NIH ImageJ software (Bethesda, Maryland, USA). All statistical analyses were performed in Statistica Version 14 (TIBCO Software Inc., CA, USA), and differences were considered significant at $P < 0.05$.

Acknowledgement

We want to thank our GITAM University, Hyderabad, for the Seed grant (Ref: F.No 2022/0174) funding to carry out the synthesis and modelling studies. The biological part of the study was supported by infrastructural projects (CZ-OPENSCREEN – LM2023052; EATRIS-CZ – LM2023053), the projects National Institute for Cancer Research (Project No. LX22NPO5102) and National Institute for Neurological Research (Project No. LX22NPO5107) - Funded by the European Union - Next Generation EU from the Ministry of Education, Youth and Sports of the Czech Republic (MEYS).

Conflict of interest statement

The authors declare no conflict of financial interests.

Data availability statement

The data that support the findings of this study are available from the corresponding authors upon reasonable request.

References

1. Carnero Contentti E, Correale J. Bruton's tyrosine kinase inhibitors: a promising emerging treatment option for multiple sclerosis. *Expert Opin Emerg Drugs*. 2020;25(4):377-381. doi:10.1080/14728214.2020.1822817
2. Krause G, Hassenrück F, Hallek M. Cell line-based assessment of BTK inhibitors. *Br J Pharmacol*. 2020;177(9):2163-2165. doi:10.1111/bph.14948
3. Salim K, Bottomley MJ, Querfurth E, et al. Distinct specificity in the recognition of phosphoinositides by the pleckstrin homology domains of dynamin and Bruton's

tyrosine kinase. *EMBO J.* 1996;15(22):6241-6250. doi:10.1002/j.1460-2075.1996.tb01014.x

4. Nore BF, Vargas L, Mohamed AJ, et al. Redistribution of Bruton's tyrosine kinase by activation of phosphatidylinositol 3-kinase and Rho-family GTPases. *Eur J Immunol*. 2000;30(1):145-154. doi:10.1002/1521-4141(200001)30:1<145:AID-IMMU145>3.0.CO;2-0
5. Wen T, Wang J, Shi Y, Qian H, Liu P. Inhibitors targeting Bruton's tyrosine kinase in cancers: drug development advances. *Leukemia*. 2021;35(2):312-332. doi:10.1038/s41375-020-01072-6
6. Tasso B, Spallarossa A, Russo E, Brullo C. The development of btk inhibitors: A five-year update. *Molecules*. 2021;26(23). doi:10.3390/molecules26237411
7. Ph D, Burger JA, Ph D, et al. NIH Public Access Author Manuscript N Engl J Med. Author manuscript; available in PMC 2014 January 04. Published in final edited form as: N Engl J Med. 2013 July 4; 369(1): 32–42. doi:10.1056/NEJMoa1215637. Targeting BTK with Ibrutinib in Relapsed Chronic. *N Engl J Med*. 2013;369(1):32-42. doi: 10.1056/NEJMoa1215637.Targeting
8. Syed YY. Zanubrutinib: First Approval. *Drugs*. 2020;80(1):91-97. doi:10.1007/s40265-019-01252-4
9. Barf T, Covey T, Izumi R, et al. Acalabrutinib (ACP-196): A covalent Bruton tyrosine kinase inhibitor with a differentiated selectivity and in vivo potency profile. *J Pharmacol Exp Ther*. 2017;363(2):240-252. doi:10.1124/jpet.117.242909
10. 2-Indolinone a versatile scaffold for treatment of cancer: A patent review (2008-2014). *Expert Opin Ther Pat*.2016; 26(2):149-173. doi:10.1517/13543776.2016.1118059
11. Khetmalis YM, Shivani M, Murugesan S, Chandra Sekhar KVG. Oxindole and its derivatives: A review on recent progress in biological activities. *Biomed Pharmacother*. 2021;141(March):111842. doi 10.1016/j.biopha.2021.111842
12. Kaur M, Singh M, Chadha N, Silakari O. *Oxindole: A Chemical Prism Carrying Plethora of Therapeutic Benefits*. Vol 123. Elsevier Ltd; 2016. doi: 10.1016/j.ejmech.2016.08.011
13. Indolinones as Promising Scaffold as Kinase Inhibitors: A Review. *Mini-Reviews Med Chem*. 2012;12(2):98-119. doi:10.2174/138955712798995039
14. Sun L, Tran N, Tang F, et al. Synthesis and biological evaluations of 3-substituted indolin-2-ones: A novel class of tyrosine kinase inhibitors that exhibit selectivity toward

particular receptor tyrosine kinases. *J Med Chem*. 1998;41(14):2588-2603. doi:10.1021/jm980123i

15. M. Krug, A. Hilgeroth, Recent advances in the development of multi-kinase inhibitors, Mini Rev. Med. Chem. 8 (2008) 1312e1327, https://doi.org/ 10.2174/138955708786369591
16. L.Q. Chow, S.G. Eckhardt, Sunitinib: from rational design to clinical efficacy, J. Clin. Oncol. 25 (2007) 884e896, https://doi.org/10.1200/JCO.2006.06.3602
17. London CA, Malpas PB, Wood-Follis SL, et al. Multi-center, placebo-controlled, double-blind, randomized study of oral toceranib phosphate (SU11654), a receptor tyrosine kinase inhibitor, for the treatment of dogs with recurrent (either local or distant) mast cell tumor following surgical excision. *Clin Cancer Res*. 2009;15(11):3856-3865. doi:10.1158/1078-0432.CCR-08-1860
18. Flaherty KR, Wells AU, Cottin V, et al. Nintedanib in progressive interstitial lung diseases: data from the whole INBUILD trial. *Eur Respir J*. 2022;59(3):1-9. doi:10.1183/13993003.04538-2020
19. Jörg M, Kaczor AA, Mak FS, et al. Investigation of novel ropinirole analogues: Synthesis, pharmacological evaluation, and computational analysis of dopamine D2 receptor functionalized congeners and homobivalent ligands. *Medchemcomm*. 2014;5(7):891-898. doi:10.1039/c4md00066h
20. Mauser M, Preisack M, Karsch KR. Acute Hemodynamic Inhibitor, for Severe. 64.
21. Caley CF, Cooper CK. Ziprasidone: The fifth atypical antipsychotic. *Ann Pharmacother*. 2002;36(5):839-851. doi:10.1345/aph.1A053
22. Kauffman RF, Robertson DW, Franklin RB, et al. Indolidan: A Potent, Long-Acting Cardiotonic and Inhibitor of Type IV Cyclic AMP Phosphodiesterase. *Cardiovasc Drug Rev*. 1990;8(4):303-322. doi:10.1111/j.1527-3466. 1990.tb00398.x
23. Claußen H, Buning C, Rarey M, Lengauer T. FLEXE: Efficient molecular docking considering protein structure variations. *J Mol Biol*. 2001;308(2):377-395. doi:10.1006/jmbi.2001.4551
24. Andér M, Luzhkov VB, Åqvist J. Ligand binding to the voltage-gated Kv1.5 potassium channel in the open state - Docking and computer simulations of a homology model. *Biophys J*. 2008;94(3):820-831. doi:10.1529/biophysj.107.112045
25. S. Sestito, G. Nesi, S. Daniele, A. Martelli, M. Digiacomo, A. Borghini, D. Pietra, V. Calderone, A. Lapucci, M. Falasca, and P. Parrella, Design and synthesis of 2-oxindole based multi-targeted inhibitors of PDK1/Akt signaling pathway for the treatment of

glioblastoma multiform, Eur. J. Med. Chem. 105 (2015) 274-288.https://doi.org/10.1016/j.ejmech.2015.10.020

26. H. Guan, A. D. Laird, R. A. Blake, C. Tang, and C. Liang, Design and synthesis of aminopropyltetrahydroindole-based indolin-2-ones as selective and potent inhibitors of Src and Yes tyrosine kinase, Bioorganic Med. Chem. Lett. 14(2004) 187-190.https://doi.org/10.1016/j.bmcl.2003.09.069
27. D. V. Kravchenko, Y. A. Kuzovkova, V. M. Kysil, S. E. Tkachenko, S. Maliarchouk, I. M. Okun, K. V. Balakin, and A. V. Ivachtchenko, Synthesis, and Structure-Activity Relationship of 4-Substituted 2-(2-Acetyloxyethyl)-8-(morpholine-4-sulfonyl) pyrrolo [3, 4-c] quinoline-1, 3-diones as Potent Caspase-3 Inhibitors, J. Med. Chem. 48(2005) 3680-3683.https://doi.org/10.1021/jm048987t
28. M. H. Kim, A. L. Tsuhako, E. W. Co, D. T. Aftab, F. Bentzien, J. Chen, W. Cheng, S. Engst, L. Goon, R.R. Klein, and D. T. Le, The design, synthesis, and biological evaluation of potent receptor tyrosine kinase inhibitors, Bioorganic Med. Chem. Lett. 22 (2012) 4979-4985. https://doi.org/10.1016/j.bmcl.2012.06.029
29. I. Islam, J. Bryant, Y. L. Chou, M. J. Kochanny, W. Lee, G. B. Phillips, H. Yu, M. Adler, M. Whitlow, E. Ho, and D. Lentz, Indolinone based phosphoinositide-dependent kinase-1 (PDK1) inhibitors, Part 1: design, synthesis and biological activity, Bioorganic Med. Chem. Lett. 17 (2007) 3814-3818. https://doi.org/10.1016/j.bmcl.2007.04.071
30. C. W. Liu, C. L. Lai, Y. H. Lin, L. W. Teng, S. C. Yang, W.Y. Wei, S. F. Lin, J.Y. Yang, H. J. Huang, R. W. Wang, and C. C. Chiang, Design and synthesis of pyrrole–5-(2, 6-dichloro benzyl) sulfonylindolin-2-ones with C-3′ side chains as potent Met kinase inhibitors, RSC Advances, 4 (2014.) 58990-58998. https://doi.org/10.1039/C4RA08720H
31. S. Mamand, R.L. Allchin, M.J. Ahearne, S.D. Wagner, Comparison of interleukin-2-inducible kinase (ITK) inhibitors and potential for combination therapies for T-cell lymphoma, Sci. Rep. 8 (2018) 14216–14216. https://doi.org/10.1038/s41598-018-32634-5
32. Y. Chu, S. Lee, T. Shah, C. Yin, M. Barth, R. R. Miles, J. Ayello, E. Morris, L. Harrison, C. Van de Ven, P. Galardy, S. C. Goldman, M. S. Lim, M. Hermiston, L. M. McAllister-Lucas, L. Giulino-Roth, S. L. Perkins, M. S. Cairo, OncoImmunology 2019, 8, e1512455.
33. Pastwa E, Somiari RI, Malinowski M, Somiari SB, Winters TA. In vitro non-homologous DNA end joining assays--the 20th anniversary. Int J Biochem Cell Biol. 2009

Jun;41(6):1254-60. doi: 10.1016/j.biocel.2008.11.007.

34. Ping L, Ding N, Shi Y, Feng L, Li J, Liu Y, Lin Y, Shi C, Wang X, Pan Z, Song Y, Zhu J. The Bruton's tyrosine kinase inhibitor ibrutinib exerts immunomodulatory effects through regulation of tumor-infiltrating macrophages. Oncotarget. 2017 Jun 13;8(24):39218-39229. doi: 10.18632/oncotarget.16836.
35. Bender AT, Gardberg A, Pereira A, et al. Ability of Bruton's tyrosine kinase inhibitors to sequester Y551 and prevent phosphorylation determines potency for inhibition of Fc receptor but not B-cell receptor signaling. *Mol Pharmacol*. 2017;91(3):208-219. doi:10.1124/mol.116.107037
36. Sterling T, Irwin JJ. ZINC 15 - Ligand Discovery for Everyone. *J Chem Inf Model*. 2015;55(11):2324-2337. doi:10.1021/acs.jcim.5b00559
37. Dallakyan, S., Olson, A. J., Small-Molecule Library Screening by Docking with PyRx. *Methods Mol. Biol.*2015. https://doi.org/10.1007/978-1-4939-2269-7_19.
38. Daina A, Michielin O, Zoete V. SwissADME: A free web tool to evaluate pharmacokinetics, drug-likeness and medicinal chemistry friendliness of small molecules. *Sci Rep*. 2017;7(October 2016):1-13. doi:10.1038/srep42717
39. Veber DF, Johnson SR, Cheng HY, Smith BR, Ward KW, Kopple KD. Molecular properties that influence the oral bioavailability of drug candidates. *J Med Chem*. 2002;45(12):2615-2623. doi:10.1021/jm020017n
40. (a) Desmond Molecular Dynamics System, Schrödinger Release 2020-1; D. E. Shaw Research: New York, 2020. (b) Maestro-Desmond Interoperability Tools; Schrödinger: New York, 2020
41. B. Grüner, J. Brynda, V. Das, V. Šícha, J. Štěpánková, J. Nekvinda, J. Holub, K. Pospíšilová, M. Fábry, P. Pachl, V. Král, M. Kugler, V. Mašek, M. Medvedíková, S. Matějková, A. Nová, B. Lišková, S. Gurská, P. Džubák, M. Hajdúch, P. Řezáčová, Metallacarborane Sulfamides: Unconventional, Specific, and Highly Selective Inhibitors of Carbonic Anhydrase IX, J. Med. Chem. 62 (2019) 9560–9575. https://doi.org/10.1021/acs.jmedchem.9b00945